Environmental Science & Technology

Article

pubs.acs.org/est

Mixing and Reaction Kinetics in Porous Media: An Experimental Pore Scale Quantification

Pietro de Anna,[†,‡] Joaquin Jimenez-Martinez,[†] Hervé Tabuteau,[§] Regis Turuban,[†] Tanguy Le Borgne,[†] Morgane Derrien,[†] and Yves Méheust*[,†]

[†]Géosciences Rennes, UMR 6118, CNRS, Université de Rennes 1, Rennes, France

[‡]Massachusetts Institute of Technology, Boston, Massachusetts, United States

[§]IPR, Université Rennes 1 - CNRS, UMR 6251, Campus Beaulieu, F-35042 Rennes, France

Supporting Information

ABSTRACT: We propose a new experimental set up to characterize mixing and reactive transport in porous media with a high spatial resolution at the pore scale. The analogous porous medium consists of a Hele-Shaw cell containing a single layer of cylindrical solid grains built by soft lithography. On the one hand, the measurement of the local, intrapore, conservative concentration field is done using a fluorescent tracer. On the other hand, considering a fast bimolecular reaction $A + B \rightarrow C$ occurring as A displaces B, we quantify the rate of product formation from the spatially resolved measurement of the pore scale reaction rate, using a chemiluminescent reaction. The setup provides a dynamical measurement of the local concentration field over 3 orders of magnitude and allows investigating a wide range of Péclet and Damköhler numbers by varying the flow rate within the cell and the local reaction rate. We use it to study the kinetics of the reaction front between A and B. While the advection-dispersion (Fickian) theory, applied at the continuum scale, predicts a scaling of the cumulative mass of product C as $M_C \propto \sqrt{t}$, the experiments exhibit two distinct regimes in which the produced mass M_C evolves faster than the Fickian behavior. In both regimes the front rate of product formation is controlled by the geometry of the mixing interface between the reactants. Initially, the invading solute is organized in stretched lamellae and the reaction is limited by mass transfer across the lamella boundaries. At longer times the front evolves into a second regime where lamellae coalesce and form a mixing zone whose temporal evolution controls the rate of product formation. In this second regime, the produced mass of C is directly proportional to the volume of the mixing zone defined from conservative species. This interesting property is indeed verified from a comparison of the reactive and conservative data. Hence, for both regimes, the direct measurement of the spatial distribution of the pore scale reaction rate and conservative component concentration is shown to be crucial to understanding the departure from the Fickian scaling as well as quantifying the basic mechanisms that govern the mixing and reaction dynamics at the pore scale.

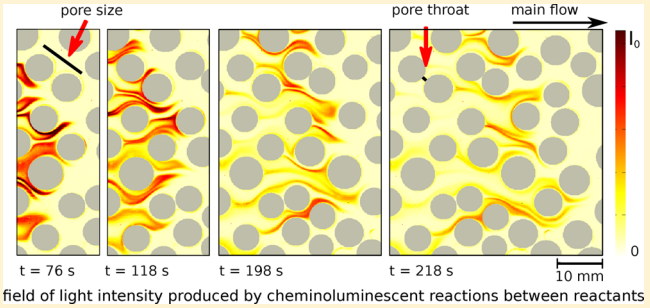

field of light intensity produced by cheminoluminescent reactions between reactants

1. INTRODUCTION

Chemical reactions govern various systems, and play a central role in to many medical and industrial applications (e.g., reactive transport in the subsurface and biological activity in living tissues[1,2]). While in well mixed reactors the kinetics are fully controlled by chemical processes, in many real situations spatial heterogeneities lead to a complex temporal evolution of the system kinetics, which depend on the transport and mixing mechanisms.[3,4] Mixing is the ensemble of processes by which substances originally segregated into different volumes of space tend to occupy the same common volume.[5] The physical processes responsible for mixing at the hydrodynamical scale are advection and molecular diffusion. In porous media, heterogeneous advection acts to spread the solutes in the local direction of the flow while diffusion tends to homogenize their spatial distribution (e.g., refs 6−10).

At the continuum scale classical descriptions of transport and mixing in porous media consist in modeling effective transport by the same theoretical framework as pore scale (diffusive) transport. The interaction between heterogeneous advection and diffusion at the pore scale are lumped in a dispersion coefficient. That dispersion coefficient describes the effective mixing processes of the solute (e.g., refs 7,11, and 12), and is obtained by upscaling of the pore scale information to the Darcy scale, for example using volume averaging (e.g., refs 13 and 14) or homogenization (e.g., ref 15) techniques. However, medium heterogeneities lead to a distortion of the solute plume that, for times smaller than the typical transport time over a

Received: July 21, 2013
Revised: November 18, 2013
Accepted: November 25, 2013

   dx.doi.org/10.1021/es403105b | Environ. Sci. Technol. XXXX, XXX, XXX−XXX

typical heterogeneity scale, increases the solute's spreading but not its degree of mixing. Thus, in general, these coupled processes of spreading and mixing need to be studied in a different manner.[10,16,17,42,43] The kinetics of reactive systems resulting from mixing in heterogeneous media can then be very different from the one derived from Fickian theories, as observed not only for porous media,[7,18−24,47] but also for a wide range of disordered and fractal systems,[25] Rayleigh-Taylor systems,[26] turbulent and chaotic flows,[1,3] homogeneous systems with the presence of stochastic fluctuations[27,28] and planar fractures.[29] Nevertheless, the impact of incomplete mixing processes and non Fickian dispersion on the effective reaction kinetics is still an open issue (e.g., ref 10).

Quantification of the degree of local mixing is a key to understanding and predicting the fate of chemical reactions whose kinetics are fast enough to be limited by mixing processes. For those systems, it is necessary to assess the local concentration fields within the porous space, at the hydrodynamic (or local) scale.[7,43] Dynamical visualization techniques have been developed to study mixing in continuous media (e.g., turbulence[30] or population dynamics of plankton in oceanic flows[1]). For porous media, that are discontinuous and characterized by the no-slip boundary conditions at solid−liquid interface, averaged concentration fields have been often evaluated experimentally through the Beer−Lambert law and colorimetry techniques applied to the light that has traveled through a bead pack representing an analogous porous medium (e.g., refs 7 and 31). The concentration of transported fluorescent colloids has also been inferred from their measured fluorescence (e.g., ref 18). Those techniques quantify the local concentration fields averaging over several pore size and, thus, cannot capture the incomplete mixing eventually present within the pores. Few experimental techniques have been developed to measure the local concentration fields and mass of reaction product (e.g., ref 19) in steady state conditions within the pores.[42] The main goal of the present work is to develop a method to perform dynamical pore scale measurements of local concentration fields and reaction rates. We thus measure the kinetics of an irreversible fast bimolecular reaction $A + B \rightarrow C$ taking place at the front between the reactants, one displacing the other, in a ($2d$) porous medium.

The analogous porous medium consists of a Hele-Shaw cell containing a single layer of cylindrical solid grains. The radii and positions of the grains along the plates are fully controlled: by using a technique common in microfluidics, we reproduce a numerical model defined at will. To assess the local concentration field of a passive scalar we consider a fluorescent tracer and we relate the local concentration to the measure of the light emitted by the stimulated tracer via a calibration process with known concentrations. To quantify the local kinetics of a mixing-limited bimolecular irreversible reaction $A + B \rightarrow C$, we resort to the fast chemiluminescent reaction described by Jonsson and Irgum:[32] for each reaction of a molecule of A with a molecule of B, a photon is emitted. The amount of light detected per unit time is, thus, proportional to the amount of reactions that have taken place. We show the relationship between the rate of product formation and the local mixing properties of the reactants, which are controlled by transport within the pores of the considered heterogeneous medium. The assessments of (i) local mixing and (ii) rate of product formation are done in two independent experiments. The findings from the two experiments, which are respectively the time evolution of the mixing volume and that of global rate of product formation, are successfully related to each other. Note that the extrapolation of the results obtained from micromodel experiments to the field is not direct in general. However, this represents a first modeling step in the development of a theoretical framework that shall quantify the impact of incomplete mixing conditions on reaction kinetics. This will provide scaling laws linking the microscale processes to the Darcy scale behavior, which is relevant to large scale modeling and applications (e.g., ref 10).

2. THEORETICAL FRAMEWORK FOR MIXING AND REACTION AT THE PORE SCALE

We consider a $2d$ medium composed of a polydispersed population of n_g randomly distributed circular grains with mean porosity ϕ. Its geometry is characterized by two length scales, the average pore throat h and the average pore size ξ (see figure in the first page). The former represents the smaller gap where a solute plume is forced to pass, while the latter is the average distance between two consecutive pore throats connected by the flow.

The flow of an incompressible fluid is described by its local velocity field $\mathbf{v}$, which is given by the continuity equation (mass conservation), $\nabla \cdot \boldsymbol{v} = \mathbf{0}$ and the momentum conservation, that is, the Navier−Stokes equation. We assume that the $2d$ porous medium is horizontal: the flow velocities are parallel to the horizontal plane and, thus, gravity does not impact them. We define the Reynolds number as $Re = \overline{v}h/\nu$, where ν is the kinematic viscosity of the fluid and $\overline{v}$ is the average flow velocity. It compares the characteristic ratio of the inertial forces in the longitudinal direction (within the pores) to the viscous forces that tend to homogenize momentum in the transverse direction (within the pore throats), for the flow of a Newtonian fluid. At low Reynolds numbers, typical of porous media, the momentum conservation for stationary conditions leads to the Stokes (laminar) flow. As a consequence of the no-slip boundary conditions at the grain walls, the velocity field of a liquid flowing through a porous medium is typically characterized by the existence of a braided network of preferential flow paths in channels, as well as low velocity or stagnation zones (e.g., ref 22).

The medium of volume V is initially saturated with a solution B, with a spatially homogeneous concentration c_0. At time $t = 0$, another solution A, also of uniform concentration c_0, starts to be injected continuously through the inlet boundary ($x = 0$). The two solutions A and B are fully miscible, and their contact front coincides initially with the inlet boundary (grains excluded), of length l_0. As solutions are transported in the medium, at the front between A and B, solution mixing takes place. The reaction between the chemicals A and B is considered bimolecular and irreversible.

We define the Péclet number by $Pe = \overline{v}(h/2)^2/(2D\xi)$. It is the ratio of the characteristic diffusion time over half a pore throat $\tau_D = (h/2)^2/(2D)$ to the characteristic advection time over a typical pore length $\tau_a = \xi/\overline{v}$. The reaction time scale is defined by the kinetics in well-mixed conditions $\tau_r = 1/(c_0 k)$.[33] The ratio of advection to reaction time scales is the Damköhler number $Da = \tau_a/\tau_r$. We consider the case of a reaction that is quasi-instantaneous with respect to advective mechanisms: $Da \gg 1$. In other words, once the reactants are locally mixed, they are chemically depleted in a very short time and reactions stop: only the occurrence of further mixing will allow reactions to take place again.

dx.doi.org/10.1021/es403105b | Environ. Sci. Technol. XXXX, XXX, XXX−XXX

A global measure of the chemical kinetics can be given in terms of the temporal scaling of the total mass of C present in the system at instant t:

$$M_C(t) = \int_V \mathrm{d}\boldsymbol{x} c_C \tag{1}$$

Well Mixed Reactant. Classical approaches consider A and B well mixed within the pores and consequently describe transport at the continuum scale as one-dimensional along the main flow direction (x).[34] In this framework the solute dispersion is described in terms of concentration fields $\overline{c}_i$ that are averaged over the elementary representative volume, larger than a single pore. The time evolution of these locally averaged concentrations undergoing reactions and transport is then described by a unidimensional advection-dispersion-reaction equation.[14] The average concentration is then advected by the constant Darcy velocity (that is, the fluid velocity defined at the continuum scale) and follows a Fickian spreading described in terms of an effective dispersion coefficient D^* that is the sum of the molecular diffusion coefficient and of the longitudinal hydrodynamic dispersion coefficient. Assuming that the support volume, larger than the single pore, is well mixed, the reaction rates are given by the mass action law $r_i^* = -k\overline{c}_A\overline{c}_B$ for $i = A, B$ and $r_C^* = -k\overline{c}_A\overline{c}_B$.[7,9,10] In this framework, the total mass of C present at instant t in the system is [7]

$$M_C(t) = c_0\sqrt{\frac{2\sigma^2}{\pi}} = c_0\sqrt{\frac{4D^*t}{\pi}} \tag{2}$$

where $\sigma^2 = 2D^*t$ is the spatial variance of a solute plume undergoing Fickian conservative transport. The nature of such a Fickian scaling law is intimately related to the complete mixing condition assumed at the pore scale. To capture, describe and predict the deviation of real systems from the model of eq 2, we shall assume that the support scale at which the transported chemicals are well mixed is much smaller than the pore scale.

Imperfectly Mixed Reactants. As discussed in ref 38 and summarized in the following, the global kinetics of the system is determined by the evolution of the mixing interface between the two chemicals. This interface Ξ between A and B is stretched by the flow field heterogeneity and develops a lamella-like topology[5,35−37] (see also the case of a conservative tracer transported in a heterogeneous porous medium as in Figure 2). A recent numerical study on pore scale mixing has shown that until those lamellae start interacting with each other, the length Σ of Ξ evolves linearly in time as $l_0(1 + \gamma t)$, where l_0 is its initial length and γ the so-called stretching rate.[38] Since the considered reaction is fast compared to transport mechanisms, the mass of A that by diffusion crosses the interface instantaneously reacts to form C, whose kinetics follows

$$\frac{\mathrm{d}M_C(t)}{\mathrm{d}t} = D\int_\Xi |\nabla c_A|\mathrm{d}\Sigma \approx Dl_0c_0\frac{(1+\gamma t)}{s(t)} \tag{3}$$

where $\Sigma = l_0(1+\gamma t)$ is the length of the interface Ξ, s its width and $|\overline{\nabla c}| \sim c_0/s$ is the average gradient across the reactants interface. The dynamics of s is controlled by the competition between stretching and diffusion:

$$s = s_0\sqrt{\frac{3\beta - 2 + 2(1+\gamma t)^3}{3\beta(1+\gamma t)^2}} \tag{4}$$

with $\beta = (s_0^2\gamma)/D$ and $s_0 = s(0)$, as discussed in refs 39 and 38. The lamellae width s decreases until compression and diffusive growth equilibrate: afterwards, the width s grows diffusively as $s \propto \sqrt{t}$.

The behavior described by eqs 3 and 4 is in fact valid until the time t^* at which the lamellae of the interface Ξ begin to interact with each other by diffusion. Their coalescence process leads to the formation of aggregate lamellae bundles,[37] so that the evolution of the interface length Σ is no longer linear in time. In this coalescence regime, the role of individual lamella is no longer dominant and the rate of product formation is simply controlled by the growth of the mixing volume V_m, defined as the portion of the system where a conservative component $c_R = c_A + c_C$ transported by the flow varies between the injected value and zero:[38]

$$M_C(t) \propto V_m \tag{5}$$

3. MATERIALS AND METHODS

3.1. Porous Medium Design: Use of the Soft Lithography Technique. We have prepared a synthetic $2d$ porous medium containing $n_g = 244$ grains, of size $S = 160$ mm in the longitudinal (main flow) direction and 100 mm in the transverse one, and characterized by a porosity $\phi = 0.55$ (see inset of Figure 1a). The device used to model the described porous medium is a Hele-Shaw cell consisting of two parallel transparent plates separated by cylindrical impermeable pillars, representing the grains of the porous medium. To build this device, we use the lithographic technique described in references 40 and 41 where two rectangular glass plates of the same size are superposed and positioned with a uniform separation distance a. Note that techniques aimed at building a $2d$ porous medium with precise given geometric characteristics have been used earlier,[44,45] but soft lithography, developed in the last 10 years mostly in the field of microfluidics, is of much easier use since it does not require a laser nor the motors to drive the photochemical reactor with high accuracy. A mask with the negative image of the chosen geometry is printed at a high resolution, here 128 000 dots per inch (DPI), on a transparent film (photomask). The porous space is represented by a single black cluster containing transparent disks that correspond to the grains. This film is placed on top of the two glass plates, the space between which is filled with a UV-sensitive glue. This glue, Norland Optical Adhesive 81, is sensitive to the entire range of long wavelength from 320 to 400 nm, with a peak sensitivity around 365 nm. A collimated light source (ThorLabs M365L2) that emits a UV beam of wavelengths limited to a sharp window peaked at 365 nm at 1 mW, is placed at a distance of 23 cm from the two glass plates and along a direction perpendicular to the mask (see Figure 1a inset). Irradiating the glue in between the glass plates through the photomask for a controlled time results in photo-polymerization of the glue in the regions where the UV light has been allowed to pass, as shown in Figure 1a. After flooding out the liquid glue remaining in the porous space, we obtain solid cylindrical grains consisting of a hard polymer. This technique provides full control on the geometry of the produced medium (here, the position and size of the cylinders).

Placing the UV source at a distance of 23 cm from the target, we measured a homogeneous power per unit surface of 0.6 ± 0.1 mW/cm^2 over an area of 15×15 cm^2. In order to obtain cylinders with sharp boundaries, the UV-light exposure time τ_{exp} was optimized: for the thickness $a = 1$ mm exposed to a UV

dx.doi.org/10.1021/es403105b | Environ. Sci. Technol. XXXX, XXX, XXX−XXX

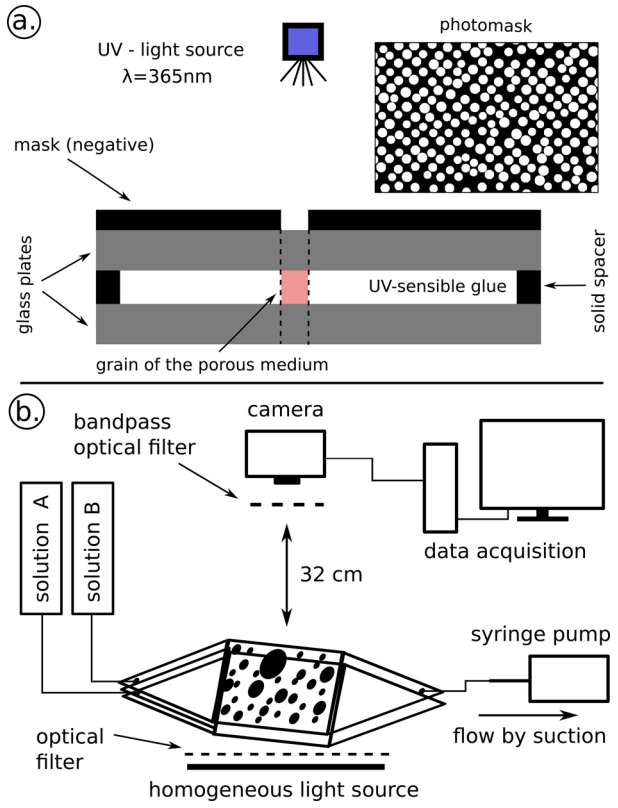

Figure 1. a. Principle of the soft lithography technique. The two glass plates are separated by a distance a = 1 mm. The photomask (inset) is placed on top of the two plates. The space between them is filled with a liquid UV-sensitive glue. The light coming from the collimated 365 nm UV source passes through the transparent disks in the mask, polymerizing the glue and giving rise to solid grains. b. A scheme of the experimental setup. A solution A is continuously injected in the porous medium saturated with a solution B through suction by a syringe pump. A homogeneous radiation of light excites the fluorescent tracer transported within the pores. A first filter in between the light source and the cell removes all wavelengths that are typical of the fluorescent emission. A second filter in front of the camera selects only the light emitted by the tracer. For the quantification of rate of product formation we use the same setup, removing the light source and the optical filters.

radiation dose of 0.6 ± 0.1 mW/cm^2, we obtained τ_{exp} = 95 s. The cure time τ_{exp} is dependent on the needed dose of radiation and thus on the light intensity and the thickness of the glue, which in our case coincides with the distance a between the glass plates. The cure time is also slightly dependent on the age of the glue. Thus, for every lithography process that was carried out, τ_{exp} was reoptimized.

Once the grains are produced in between the glass plates, two opposite sides of the chamber are sealed using the same glue as above. The other two opposite sides will constitute the inlet and the outlet of the set up. The injection system is shown schematically in Figure 1b: via two inlet points on two separate superposed prisms (one for each injected substance), the flow is carried out homogeneously in the chamber. In this way the two different injected solutions will mix only inside the porous medium. The flow velocities within such a chamber placed horizontally are not impacted by body forces, and are consequently parallel to the plane of the chamber. They are controlled locally, due to the no-slip boundary conditions, by the smallest distance between neighboring solid walls. In this case, the wall to wall distances that control the flow are the thickness of the Hele-Shaw cell (distance between the horizontal glass plates), a, and the widths of the pore throats, the average value of which is $h \sim 1$ mm. If the cell is very thin compared to the average pore throat, $a \ll h$, then the vertical profile of the flow will be parabolic, while in the other direction it will correspond to a plug flow[46] and the flow field heterogeneity in most of the porous volume will remain moderate. In particular, for Hele-Shaw flow the fluid shear will mostly occur in the vertical direction, except in narrow limit layers close to the cylinders' walls, so that hydrodynamic dispersion will be less efficient in the medium. To avoid this condition, we set the cell thickness to $a \simeq h$, a = 1 mm.

3.2. Characterization of Passive Scalar Transport. We impose a controlled flow rate Q between the inlet and outlet boundaries of the cell using a syringe pump (*Harvard Apparatus PHD 2000*), by suction. We use a glass syringe of 50 mL (Tomopal Inc.). Once the cell, the injection system and all the pipes have been fully saturated with clear water, a solution of Fluorescein (Fluorescein sodium salt) of concentration c_0 = 255 mg/L is injected. The injection system is schematically shown in Figure 1 b. A point injection is homogeneously transferred to the inlet opening of the chamber via two superposed prisms: one dedicated to the injection of clear water and the other to the fluorescent solution. In this way the two different injected solutions will mix only inside the porous medium.

A panel source that produces a spatially homogeneous intensity of light illuminates the porous medium from below. An optical filter (LEE 126 Mauve), positioned between the light panel and the cell, prevents wavelengths in the window $\lambda \in [505-580]$ nm from passing through. The fluorescent tracer, excited by the radiation received at λ = 494 nm, emits photons with a wavelength λ = 521 nm while relaxing to its ground state. The amount of emitted photons is proportional to the number of excited tracer molecules and, thus, to the local tracer concentration. A second filter (Edmund Optics 520 nm CWL, 10 nm Bandwidth), placed in front of a high resolution camera (an actively cooled Princeton Instruments, MegaPlus EP11000), allows only wavelengths in a sharp window with peak at λ = 520 nm ±10 nm to pass.

The camera is placed on top of the porous medium at a distance of 32 cm. We focus the optics onto the cell median horizontal plane, which is located at half the thickness of the porous medium. In the configuration used, the size of a pixel corresponds to 0.043 mm on the porous medium. In absence of fluorescent tracer no light is emitted and the associated value of the intensity detected by the camera, stored in an image, represents the background noise of our measurement. When Fluorescein is present, photons are emitted and some of them detected by the camera: the associated value is in between 0 (or the noise) and $2^{12} - 1$, since the camera has a 12-bit pixel depth. The measurement of the light intensity detected by the camera in each pixel, during the exposure time τ_{exp}, is stored in gray scale images. We take pictures every two seconds while injecting the fluorescent tracer: all images are processed and converted to images of local concentration field (averaged over the pixel size), via the calibration procedure described in detail in the Supporting Information (SI). The calibration procedure is associated to an exposure time value that remained unchanged during the experiment. With this set up the background noise in the intensity measurement is 0.66% of the maximum pixel depth (the average pixel value in the background image is 26 over 4096 channels, 12-bit). This

dx.doi.org/10.1021/es403105b | Environ. Sci. Technol. XXXX, XXX, XXX−XXX

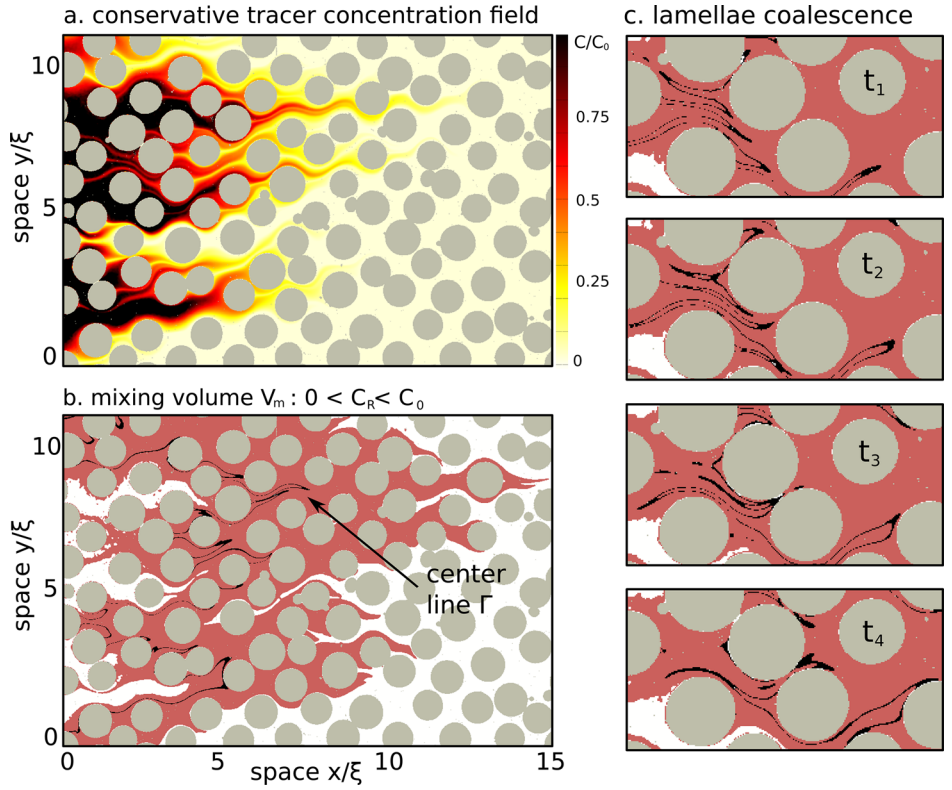

Figure 2. a. the concentration field of the conservative tracer; b. the mixing volume V_m (red area) defined as the volume of the system where $99\%c_0 > c_R > 1\%c_0$. Within the mixing volume, its center line Γ, defined as the points where $49\%c_0 > c_R > 51\%c_0$, is plotted in black. *c*. The coalescence of lamellae is represented by the merging of the centerline in four consecutive snapshots at times t_1 = 290 s, t_2 = 373 s, t_3 = 455 s, and t_4 = 538 s.

implies that the minimum concentration that can be detected, after calibration, is 0.43 mg/L, that is 0.17% of the injected concentration c_0 = 255 mg/L. Thus, this technique provides a spatially resolved detection and quantification of concentrations down to 0.2% of the injected concentration value.

3.3. Characterization of a Reactive Front from the Spatial Distribution of Local Reaction Rates. To quantify the kinetics of the front between two chemicals *A* and *B* we choose two reactants that, when mixed, produce light proportionally to the amount of reactions that take place, a property that is called cheminoluminescence. Each reaction produces a photon. To this end, we use the very fast peroxyoxalate chemiluminescence described in reference 32 where the best combination of reaction speed and intensity of the emitted light is discussed. We use bis(2,4,6-trichlorophenyl)oxalate (TCPO) under the catalytic influence of 1,8-diazabicyclo-[5,4,0]-undec-7-ene (DBU) and 1,2,4-Triazole that when combined with the fluorescent dye 3-aminofluoranthene (3−AFA) and hydrogen peroxide (H_2O_2), will start a chemiluminescent reaction and glow a fluorescent color. In order to reproduce the kinetics $A + B \rightarrow C$ we use the same molar concentration of TCPO and H_2O_2, which are the limiting species of the reaction. Following,[32] we prepare two solutions *A* and *B*. We define *A* as a mixture of a molar concentration of 0.5 mM of DBU, 5 mM of Triazole, 50 nM of 3 − AFA and 1 mM of H_2O_2. We define *B* as a solution of 1 mM of TCPO. The solvent is the same for both solutions, Acetonitrile; at 25 °C it has a dynamic viscosity $\mu = 3.4 \times 10^{-4}$ kg/(m·s), a density ρ = 0.787 kg/m^3 and thus a kinematic viscosity $\nu = 0.45 \times 10^{-4}$ m^2/s. We have successfully tested the resistance of the glue used to produce the cell to this strong solvent for more than 24 h. We assume that the diffusion coefficients of solutions *A* and *B* are identical. Since the molar masses of TCPO (448.90) and Fluorescein (376.28) are of the same order of magnitude, as well as their densities, we assume that the diffusion coefficient of TCPO is the same as the one of Fluorescein in a fluid with the same viscosity as Acetonitrile, $D = 1.6 \times 10^{-3}$ mm^2/s.

The kinetics of the considered reaction can be tuned as described in ref 32 by changing the proportion of the catalysts in the solutions *A* and *B* in order to obtain faster or slower reactions. We define t_r as the characteristic time for the reaction to reduce the emitted light by a factor 10 in a well mixed volume. As discussed in ref 32 for the chemicals chosen and the adopted molar concentrations, t_r is around 2s. In order to study a mixing limited reaction we want to impose that the Damköhler, $Da = \tau_a/\tau_r$, be much larger than 1, thus we will impose a flow rate such that the average velocity $\overline{v}$ over the average pore size ξ = 12 mm be smaller than ξ/τ_r = 6 mm/s.

For the quantification of the rate of product formation we use a sCMOS camera (the Hamamatsu ORCA flash 4.0) that is very sensible to light and has pixel resolution of 16−bit, but a smaller spatial resolution (4 megapixel) compared with the CCD camera used for the conservative tracer concentration measurements. The spatial light distribution recorded in one such picture provides a measurement of the derivative in time of the concentration of the reaction product *C*, that is, dc_C/dt. In addition, at a given time, the overall activity of the reaction can be quantified from the total light intensity detected per unit time, as

$$I(k) = \sum_{ij} P_{i,j}^{(k)}/\tau_k^{\exp} \qquad (6)$$

dx.doi.org/10.1021/es403105b | *Environ. Sci. Technol.* XXXX, XXX, XXX−XXX

where $P_{i,j}^{(k)}$ is the value of the pixel of coordinate indices (i,j) in the kth image taken and τ_k^{exp} is the exposure time of the camera for that image. This total intensity is proportional to the derivative in time of the total produced mass of the product C.

4. RESULTS AND DISCUSSION

4.1. Solute Tracer Mixing and Dispersion. We measure the evolution of the local concentration field $c_R(x,t)$ of a fluorescent tracer inside the synthetic porous medium. An example of the concentration field measured at a given time is shown in Figure 2.a, and the longitudinal projections of the concentration field are shown in inset of Figure 3 at four

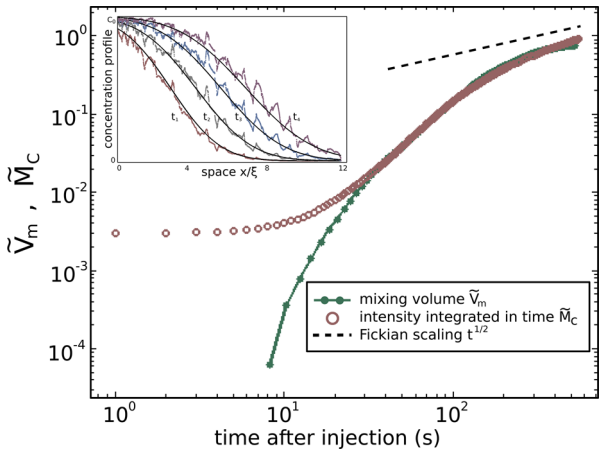

Figure 3. The solid line connecting the dots represents the temporal scaling of the mixing volume $\tilde{V}m = \varepsilon V_m$ that has been rescaled by the arbitrary constant ε, for an imposed flow rate Q = 8.3 mm^3/s. In the coalescence regime it scales as the temporal evolution of the total mass produced by the reaction, rescaled by its value at the end of the experiment: $\tilde{M}_C$, shown as circles. This quantity is given by the temporal integration of eq 6. Note that the mixing volume is rescaled by an arbitrary constant to match the two curves. In the inset: longitudinal projections of the concentration field of the injected conservative tracer (Fluorescein) at four times: t_1 = 290 s, t_2 = 373 s, t_3 = 455 s and t_4 = 538 s. The smooth solid lines represent the analytical solution of eq 7 at the same times.

equispaced times. The data can be fitted well with the analytical solution of a unidimensional advection-dispersion equation (e.g., ref 34):

$$c_R(x,t) = \frac{c_0}{2}\mathrm{erfc}\left(\frac{x-\overline{v}t}{\sqrt{2D^*t}}\right) \quad (7)$$

where the measured average velocity of the front, corresponding to the Darcy velocity, is $\overline{v}$ = 0.21 mm/s, and the dispersion coefficient has been fitted to D^* = 2.15 mm^2/s. A similar result was obtained in ref 7 for conservative transport.

We then measure the mixing volume V_m defined as the ensemble of pixels where the associated value of the concentration field is in between 1% and 99% of c_0. The mixing volume associated to the concentration field snapshot of Figure 2.a is shown in Figure 2.b. The temporal evolution of the mixing volume rescaled by an arbitrary constant, $\tilde{V}_m = \varepsilon V_m$, is shown as a solid line connecting dots in Figure 3. A comparison with the Fickian behavior $t^{1/2}$ shows that mixing is clearly non Fickian over the range of time scales investigated. Thus, the mixing volume cannot be predicted from the knowledge of dispersive spreading alone, as previously observed by the authors of refs 7 and 31 with measurements performed at the Darcy scale. This can be also observed qualitatively from the images of the concentration field in Figure 2.a, which shows that the pores are far from being well mixed.

Superimposed on the image of V_m in Figure 2.b, we have represented by a solid curve the center line Γ of V_m, defined as the ensemble of points at which the concentration field c_R has values between 49% and 51% of c_0. In the right column of Figure 2, we have represented four zoomed snapshots of V_m and its center line Γ. The evolution of this line illustrates the deformation induced by the flow heterogeneity, which creates stretched lamellae that are initially well-defined and separated. As time increases, lamellae undergo a coalescence process to form a larger lamellae bundle. This process is qualitatively similar to that observed in heterogeneous Darcy scale permeability fields.[37] In the following we quantify the impact of these phenomena (lamella stretching and coalescence) in the case where a reaction takes place at the front between two displacing chemicals.

4.2. Control of a Reaction Front by the Dynamics of Mixing. We now present the results obtained from the reactive transport experiments that we performed in the two-dimensional porous medium described in Section 3.1. To test and validate the technique, we have assessed the kinetics of the aforementioned chemicals A and B in a configuration for which the advection-dispersion-reaction equation and eq 2 are a valid description: a cell of thikness a = 1 mm without obstacles, representing a simple planar fracture (see Figure 4). The details of this validation can be found in the SI.

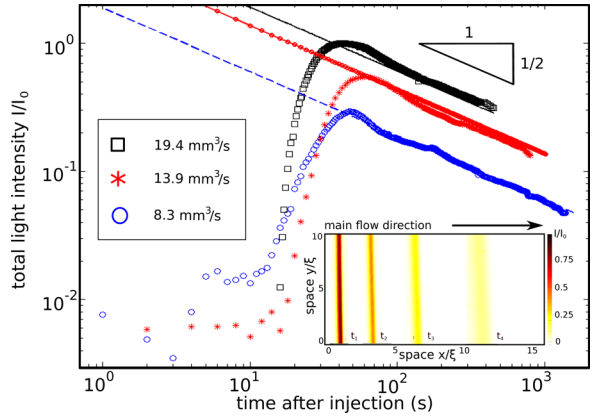

Figure 4. Temporal evolution of the total light intensity as defined in eq 6. The characteristic diffusion time over the half cell aperture, $t_T = (a/2)^2/(2D)$ = 83.3 s, defines the beginning of the Taylor dispersion regime (the impact of vertical gradients on longitudinal dispersion are becoming negligible): it is independent of the imposed flow rate. In the inset: four snapshots of the light intensity detected by the camera at four consecutive times (t_1 = 130s, t_2 = 230s, t_3 = 430s and t_4 = 737s) for flow Q = 8.3 mm^3/s during the reactive front displacement along the planar fracture. See also the SI.

The main physical quantities that characterize these reactive transport experiments performed in the analogous porous medium are summarized in Table 1.

Initially, fingers of the invading chemical penetrate channels between grains. The reaction takes place at the interface Ξ between the two chemicals, whose perimeter is represented in the inset of Figure 6, that is, at the boundaries of the fingers. The interface Ξ is stretched by the flow field heterogeneity, and develops a lamella-like topology. As mentioned previously, this

dx.doi.org/10.1021/es403105b | Environ. Sci. Technol. XXXX, XXX, XXX−XXX

Table 1. Experimental Conditions of the Conservative and Reactive Experiments, for the Three Investigated Flow Rates: Flow Q, Mean Velocity $\overline{v}$, the Reynolds (c conservative and r reactive case), Péclet, and Damköhler Numbers

Q [mm^3/s]	$\overline{v}$ [mm/s]	Re_c [-]	Re_r [-]	Pe [-]	Da [-]
8.3	0.08	0.08	0.0002	0.54	72
27.8	0.28	0.28	0.0006	1.8	21.6
83.3	0.83	0.83	0.002	5.4	7.2

type of mixing process is known to occur under advection by heterogeneous flows.[5,35−37] At larger times, the lamellae coalesce by diffusion and the reaction occurs over a more dispersed area of the porous space. We quantify the rate of product formation at the heterogeneous front between the two chemicals by measuring the total intensity I, as defined by eq 6, of the light detected per unit time.

The temporal scaling of the light intensity I is shown in Figure 5 (symbols) for three imposed flow rates Q_1 = 8.3 mm^3/s, Q_2 = 27.8 mm^3/s and Q_3 = 83.3 mm^3/s. At all times the temporal scaling of the measured total intensity I is significantly different from the $t^{-1/2}$ behavior predicted by the model of ref 7, which has been validated for the Taylor dispersion case (Hele-Shaw cell without solid grains inside). As suggested by eq 3, in the lamellae stretching regime the reaction rate is directly related to the length Σ_i of the interface Ξ between the two chemicals. We measure the temporal evolution of Σ_i by computing, for each recording time, the perimeter of the area where the reaction takes place, that is, where light is detected, as shown in the inset of Figure 6. This has been done for each investigated flow rate Q_i (i = 1, 2, 3). When lamellae are separated and independent, the interface length Σ grows approximately linearly: $\Sigma_i = l_0(1 + \gamma_i t)$. Figure 6 shows the temporal scaling of the measured $\Sigma_i - \Sigma_i(0)$ for the three flow rates; its temporal behavior is well fitted by $l_0\gamma_i t$, where the stretching rate is fitted for the flow rate Q_2 (γ_2 = 0.6 s^{-1}) and the stretching rates for the two other flow rates are inferred according to $\gamma_1 = (Q_1/Q_2)\gamma_2$ and $\gamma_3 = (Q_3/Q_2)\gamma_2$. The transition

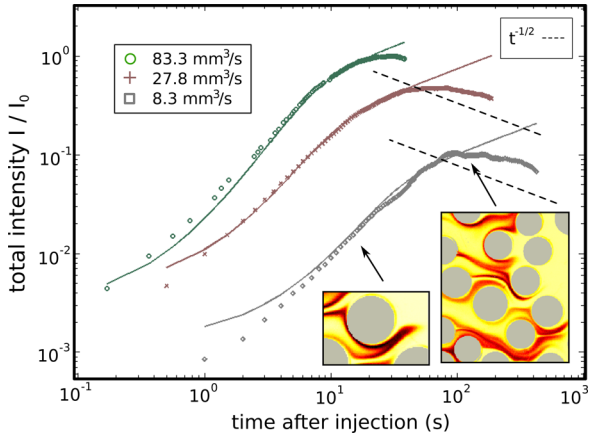

Figure 5. Temporal evolution of the global rate of product formation for three imposed flows. Before the diffusive coalescence of lamellae takes place, the model described by eq 3 predicts the experimental data well. At larger times the rate of product formation decays slower than the Fickian scaling $t^{-1/2}$. In this regime the temporal evolution of M_C is well predicted by the scaling of the mixing volume V_m of a conservative solute, measured independently (see Figure 3).

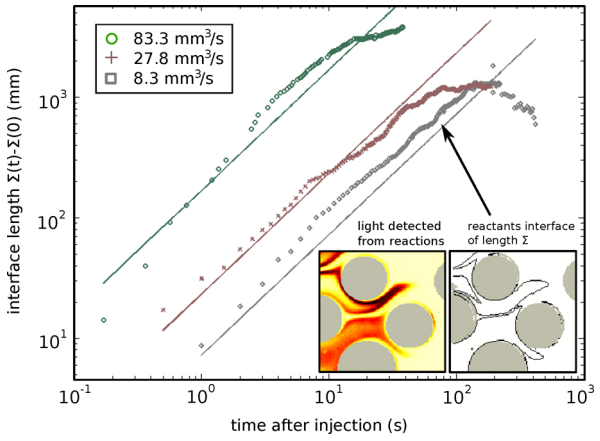

Figure 6. The dots represent the temporal evolution of $\Sigma - \Sigma(0)$, where Σ is the length of the interface between the chemicals A and B, measured as the perimeter of the image portion where light is detected. For each investigated flow rate Q_i (i = 1,2,3) and for times smaller than t^* = 105, 38, and 17 s, respectively, $\Sigma_i - \Sigma(0)$ scales as $l_0\gamma_i t$ (lines). In the inset we show a zoomed-in snapshot of the light detected at the front between the two injected chemicals and of the corresponding perimeter of the zone where reactions take place.

times between the linear and non linear regime for Σ_i are t_1^* = 105 s, t_2^* = 38s and t_3^* = 17s. In this linear stretching regime, the kinetics of the front (symbols in Figure 5) is fully controlled by line stretching and the lamellae width evolution, as described by eq 3 (the solid lines in Figure 5). Note that the value of c_0 is fitted from our measure for the flow 8.3 mm^3/s and used for all the other experiments (without any other fitting parameter). Note also that when replicating an experiment in the same flow conditions, we obtain slightly different spatial configurations of the detected light due to the fact that our control on the initial conditions is not perfect. However, the overall behavior (as quantified by the temporal evolution of the global rate of product formation) results to be the same.

At later times ($t > t^*$), the interface length Σ stops growing linearly and the rate of product formation slows down. Note that in this coalescence regime the temporal scaling of the kinetics decays more slowly than the $t^{-1/2}$ behavior observed in the Taylor-dispersion case. As stated by eq 5, the scaling of the mass production by the reaction in this coalescence regime can be well predicted by the temporal scaling of the mixing volume V_m, which is measured from independent conservative transport experiments (see Figure 3).

In summary, we have considered a situation in which two chemicals, one displacing the other, are mixed within a heterogeneous porous medium and cannot be considered well mixed at the pore scale. The kinetics of the reaction is controlled by the geometry of the interface front between the two chemicals. This geometry has a lamellae-like topology and is controlled by the dynamic competition between advective stretching and molecular diffusion. In a first regime, stretching is dominant and results in a linear growth of the interface length; in a second regime, molecular diffusion promotes the coalescence of lamellae. The global reaction rate measured with our experimental setup is in agreement with the prediction of the model described by eqs 3 and 5 for the stretching and coalescence regime,[38] respectively, that accounts for incomplete mixing at the pore scale. Particularly, in the second (coalescence) regime, the scaling is expected to be directly related to the evolution in time of the mixing volume of a

dx.doi.org/10.1021/es403105b | Environ. Sci. Technol. XXXX, XXX, XXX−XXX

conservative solute, $V_m(t)$. This is confirmed by a comparison with the $V_m(t)$ measured from an independent experiment addressing conservative transport in the same porous medium. Note that while this conservative transport experiment exhibits Fickian longitudinal dispersion, the rate of product formation shows a non-Fickian behavior characteristic of incomplete mixing at the pore scale.

The experimental technique proposed here allows for the quantification of the local rate of product formation and for the measurement of passive concentration fields at the pore scale. It can be applied to many configurations of mixing and reactive transport in porous media. The more complex three-dimensional case would lead to different reaction front geometries. However, the basic mechanisms that determine the dynamics of the chemical reaction in two dimensions, are the same basic mechanisms that control the reaction dynamics in three dimensions, where the invasion front of the displacing solute is not a diffuse line but a surface, which is stretched and compressed according to the kinematics of the local flow field. In this work we have considered the extreme case of a kinetics that can be considered instantaneous with respect to the mixing mechanisms, but the same technique can be used to study configurations where kinetics and mixing compete. In fact, using a different combination of the catalysts of the chemoluminescent reaction, it is possible to obtain a controlled slower kinetics, as described in ref 32.

■ ASSOCIATED CONTENT

Supporting Information

The Supporting Information details the calibration procedure used in this study to obtain measurement of the concentration field of the considered fluorescent tracer and the validation of the rate of product formation assessment. This material is available free of charge via the Internet at http://pubs.acs.org.

■ AUTHOR INFORMATION

Corresponding Author

*(Y.M.) E-mail: yves.meheust@univ-rennes1.fr.

Notes

The authors declare no competing financial interest.

■ ACKNOWLEDGMENTS

P.d.A. and T.L.B. acknowledge the financial support of the European Commission through FP7 ITN project IMVUL (Grant Agreement 212298) and Marie Curie ERG grant Reactive Flows (Grant Agreement Number 230947). J.J.-M. expresses his gratitude to Fondation Rennes 1 (Chaire Environment et Innovation). Y.M. gratefully acknowledges support from Rennes-Métropole through an A.I.S grant for equipment and from CNRS/INSU under grant number 786971 of the EC2CO program. Jean-Jacques Kermarrec, Pascal Rolland and Alain Faisant are gratefully acknowledged for their contribution in the design of the experiment.

■ REFERENCES

(1) Tel, T.; Demoura, A.; Grebogi, C.; Karolyi, G. Chemical and biological activity in open flows: A dynamical system approach. *Phys. Rep.* **2005**, *413*, 91−196.

(2) Seymour, J. D.; Gage, J. P.; Codd, S. L.; Gerlach, R. Anomalous fluid transport in porous media induced by biofilm growth. *Phys. Rev. Lett.* **2004**, *93*, 198103.

(3) Neufeld, Z.; Hernandez-Garica, E. *Chemical and Biological Processes in Fluid Flows: A dynamical System Approach*; Imperial College Press: London, 2010.

(4) Horsthemke, W.; Fedotov, S.; Mendez, V. *Reaction-Transport Systems*, 1st ed.; Springer: Berlin, 2010.

(5) Ottino, J. *The Kinematics of Mixing: Stretching, Chaos, And Transport*; Cambridge University Press, 1989.

(6) Jha, B.; Cueto-Felgueroso, L.; Juanes, R. Fluid mixing from viscous fingering. *Phys. Rev. Lett.* **2011**, *106*, 194502.

(7) Gramling, C. M.; Harvey, C. F.; Meigs, L. C. Reactive transport in porous media: A comparison of model prediction with laboratory visualization. *Environ. Sci. Technol.* **2002**, *36*, 2508−2514.

(8) De Wit, A. Fingering of chemical fronts in porous media. *Phys. Rev. Lett.* **2001**, *87*, 054502.

(9) Tartakovsky, A. Langevin model for reactive transport in porous media. *Phys. Rev. E* **2010**, *82*, 026302.

(10) Dentz, M.; Le Borgne, T.; Englert, A.; Bijeljic, B. Mixing, spreading and reaction in heterogeneous media: A brief review. *J. Contam. Hydrol.* **2011**, *120*−*121*, 1−17.

(11) Taylor, G. Dispersion of Soluble Matter in Solvent Flowing Slowly through a Tube. *Proc. R. Soc. A* **1953**, *219*, 186−203.

(12) Aris, R. On the dispersion of a solute in a fluid flowing through a tube. *Proc. R. Soc. A* **1956**, *253*, 67−77.

(13) Quintard, M.; Whitaker, S. Convection, dispersion, and interfacial transport of contaminants: Homogeneous porous media. *Adv. Water Resour.* **1994**, *17*, 221−239.

(14) Whitaker, S. *The Method of Volume Averaging*; Springer, 1999; Vol. *1*.

(15) Hornung, U. *Homogeneization and Porous Media*; Springer-Verlag: New York, 1997.

(16) Kitanidis, P. K. The concept of the dilution Index. *Water Resour. Res.* **1994**, *30*, 2011.

(17) Le Borgne, T.; Dentz, M.; Davy, P.; Bolster, D.; Carrera, J.; de Dreuzy, J.; Bour, O. Persistence of incomplete mixing: A key to anomalous transport. *Phys. Rev. E* **2011**, *84*, 015301.

(18) Weisbrod, N.; Niemet, M.; Selker, J. Light transmission technique for the evaluation of colloidal transport and dynamics in porous media. *Environ. Sci. Technol.* **2003**, *37*, 3694−3700.

(19) Willingham, T.; Werth, C.; Valocchi, A. Evaluation of the effects of porous media structure on mixing-controlled reactions using pore-scale modeling and micromodel experiments. *Environ. Sci. Technol.* **2008**, *42*, 3185−3193.

(20) Berkowitz, B.; Scher, H. Theory of anomalous chemical transport in random fracture networks. *Phys. Rev. E* **1998**, *57*, 5858−5869.

(21) Le Borgne, T.; Bolster, D.; Dentz, M.; de Anna, P.; Tartakovsky, A. M. Effective pore-scale dispersion upscaling with a correlated continuous time random walk approach. *Water Resour. Res.* **2011**, *47*, W12538.

(22) de Anna, P.; Le Borgne, T.; Dentz, M.; Tartakovsky, A.; Bolster, D.; Davy, P. Flow Intermittency, Dispersion and Correlated Continuous Time Random Walks in Porous Media. *Phys. Rev. Lett.* **2013**, *101*, 184502.

(23) Bijeljic, B.; Mostaghimi, P.; Blunt, M. Signature of Non-Fickian Solute Transport in Complex Heterogeneous Porous Media. *Phys. Rev. Lett.* **2011**, *107*, 204502.

(24) Sahimi, M. *Flow and Transport in Porous Media and Fractured Rock*; Wiley-VCH, 2011.

(25) Havlin, S.; Ben-Avraham, D. Diffusion in disordered media. *Adv. Phys.* **2002**, *51*, 187−292.

(26) Scagliarini, A.; Biferale, L.; Mantovani, F.; Pivanti, M.; Pozzati, F.; Sbragaglia, M.; Schifano, S. F.; Toschi, F.; Tripiccione, R. Front propagation in Rayleigh-Taylor systems with reaction. *J. Phys.: Conference Series* **2011**, *318*, 092024−1/10.

(27) Kang, K.; Redner, S. Fluctuation-dominated kinetics in diffusion-controlled reactions. *Phys. Rev. A* **1985**, *32*, 435−447.

(28) de Anna, P.; Le Borgne, T.; Dentz, M.; Bolster, D.; Davy, P. Anomalous Kinetics in Diffusion Limited Reactions Linked to Non-Gaussian Concentration PDF. *J. Chem. Phys.* **2011**, *135*, 174104.

(29) Porta, G. M.; Thovert, J. F.; Riva, M.; Guadagnini, A.; Alder, P. Microscale simulation and numerical upscaling of a reactive flow in a plane channel. *Phys. Rev. E* **2012**, *86*, 036102.
(30) Villermaux, E.; Duplat, J. Mixing is an aggregation process. *Compt. Rend. Mec.* **2003**, *91*, 18450.
(31) Oates, P. M.; Harvey, C. F. A colorimetric reaction to quantify fluid mixing. *Exp. Fluids* **2006**, *41*, 673−683.
(32) Jonsson, T.; Irgum, K. Very fast peroxyoxalate chemiluminescence. *Anal. Chim. Acta* **1999**, *400*, 257−264.
(33) Connor, K. *Chemical Kinetics*; VCH publishers, 1990.
(34) Bear, J. *Dynamics of Fluids in Porous Media*; American Elsevier, New York, 1972.
(35) Kleinfelter, N.; Moroni, M.; Cushman, J. H. Application of the finite-size Lyapunov exponent to particle tracking velocimetry in fluid mechanics experiments. *Phys. Rev. E* **2005**, *72*, 056306.
(36) Duplat, J.; Villermaux, E. Mixing by random stirring in confined mixtures. *J. Fluid Mech.* **2008**, *617*, 51−86.
(37) Le Borgne, T.; Dentz, M.; Villermaux, E. Stretching, coalescence and mixing in porous media. *Phys. Rev. Lett.* **2013**, *110*, 204501.
(38) de Anna, P.; Le Borgne, T.; Dentz, M.; Tartakovsky, A. M. Kinetics of reactive fronts in porous media. *under review* **2013**.
(39) Villermaux, E. Mixing by porous media. *Compt. Rend. Mec.* **2012**, *340*, 933−943.
(40) Harrison, C.; Cabral, J. a. T.; Stafford, C. M.; Karim, A.; Amis, E. J. A rapid prototyping technique for the fabrication of solvent-resistant structures. *Journal of Micromechanics and Microengineering* **2004**, *14*, 153−158.
(41) Cabral, J. a. T.; Hudson, S. D.; Harrison, C.; Douglas, J. F. Frontal photopolymerization for microfluidic applications. *Langmuir: the ACS journal of surfaces and colloids* **2004**, *20*, 10020−9.
(42) Rolle, M.; Eberhardt, C.; Chiogna, G.; Cirpka, O. A.; Grathwohl, P. Enhancement of dilution and transverse reactive mixing in porous media: Experiments and model-based interpretation. *Journal of Contaminant Hydrology* **2009**, *47*.
(43) Chiogna, G.; Cirpka, O. A.; Grathwohl, P.; and Massimo Rolle. Transverse mixing of conservative and reactive tracers in porous media: Quantification through the concepts of flux-related and critical dilution indices. *Water Resour. Res.*, **2011**, *47*.
(44) Bonnet, J.; Lenormand, R. Constructing micromodels for study of multiphase flow in porous-media. *Exp. Fluids* **1977**, *32*, 477−480.
(45) Didierjean, S.; Souto, H. P. A.; Delannay, R.; Moyne, C. Dispersion in periodic porous media. Experience versus theory for two-dimensional systems. *Chem. Eng. Sci.* **1997**, *52*, 1861−187.
(46) Hele-Shaw, H. S. S. author. *Trans. Instn. Nav. Archit.* **1898**, *40*, 21.
(47) Raje, D. S.; Kapoor, V. Experimental study of bimolecular reaction kinetics in porous media. *Environ. Sci. Technol.* **2000**, *34*, 1234−1239.

■ NOTE ADDED AFTER ASAP PUBLICATION

This paper was modified from the original version published on December 6, 2013 to include an additional reference and to fix a typo in Figure 2. The corrected version was published on December 10, 2013.